

CLINICAL DEVICE-RELATED ARTICLE

In vivo corrosion and damages in modular shoulder prostheses

Maria Crackau^{1,2} | Nicole Märten² | Karsten Harnisch¹ | Alexander Berth² |
Joachim Döring² | Christoph H. Lohmann² | Thorsten Halle¹ | Jessica Bertrand²

¹Institute of Materials and Joining Technology, Otto-von-Guericke University, Magdeburg, Germany

²Department of Orthopaedic Surgery, Otto-von-Guericke University, Magdeburg, Germany

Correspondence

Jessica Bertrand, Department of Orthopaedic Surgery, Leipziger Straße 44, 39120 Magdeburg, Germany.

Email: jessica.bertrand@med.ovgu.de

Abstract

Wear and corrosion at taper junctions of orthopaedic endoprotheses remain of great concern and are associated with adverse clinical reactions. Whereas tribocorrosion of hip tapers was extensively investigated, there is only little knowledge regarding the clinical performance of modular total shoulder prostheses. This retrieval study evaluated 35 modular taper junctions of anatomical shoulder explants using stereomicroscopy, confocal microscopy, as well as optical and scanning electron microscopy to determine the damage modes as well as the effects of taper topography and alloy microstructure. Among all humeral head tapers, 89% exhibited material degradation. Different overlapping wear mechanisms were identified such as plastic deformation, adhesive material transfer, microploughing, and fretting damage. Only CoCrMo cast alloy heads showed a susceptibility to electrochemically dominated fretting in comparison to CoCrMo wrought alloy. Moreover, corundum blasted stem tapers show a significantly increased incidence rate for microploughing. To date, this is the most comprehensive study on the damage types of modular taper junctions of anatomical shoulder arthroplasty proving the existence of fretting even on less weight-bearing implants. This study revealed critical fretting factors, such as the surface finish and the alloy type that are essential for the development of countermeasures that avoid any taper corrosion.

KEYWORDS

corrosion, fretting, modularity, shoulder endoprosthesis, taper

1 | INTRODUCTION

Total shoulder arthroplasties (TSA) show excellent clinical results and are more frequently implanted with a fast-growing demand (Deore, Griffiths, & Monga, 2018; Fevang, Nystad, Skredderstuen, Furnes, & Havelin, 2015; Kim, Wise, Zhang, & Szabo, 2011). The common indications for TSA are primary/secondary osteoarthritis, instability, or fractures. The rising implantation rate can be associated with the increasing variety of modular implant designs and materials that are specially adapted to different medical and individual anatomic conditions. The

modularity of anatomical prostheses allows an ideal reconstruction of the shoulder joint and kinetics. Besides an average 10-year cumulative survival rate of 90% for anatomical shoulder arthroplasties, there are cases of premature implant failure that lead to revision surgeries (National Joint Replacement Registry, 2016; Rasmussen et al., 2018; Singh, Spering, & Cofield, 2011). Reasons for revision surgery are rotator cuff failure with secondary implant failure, dislocation, periprosthetic fracture, septic and aseptic loosening. Rising TSA implantations cause increased numbers of challenging revision surgeries.

In total hip arthroplasty, the occurrence of fretting and corrosion in the modular head-neck taper junction, due to micromotion at cyclic

Maria Crackau and Nicole Märten authors contributed equally to this work.

This is an open access article under the terms of the Creative Commons Attribution-NonCommercial License, which permits use, distribution and reproduction in any medium, provided the original work is properly cited and is not used for commercial purposes.

© 2019 The Authors. *Journal of Biomedical Materials Research Part B: Applied Biomaterials* published by Wiley Periodicals, Inc.

loading, is known as mechanically assisted crevice corrosion (MACC) and is reported with prevalence rates of 3.2% up to 5% in at least one taper design (Hussey & McGrory, 2017; McGrory, MacKenzie, & Babikian, 2015). The complex mechanical and electrochemical interactions due to MACC generate ionic and particulate corrosion products that can elicit adverse local tissue reactions (ALTR). Different studies have proven that ALTR mimics infection symptoms, leads to periprosthetic tissue necrosis and is accompanied by pain and complicated revision surgeries (Meyer et al., 2012; Plummer et al., 2016). Macro- and microscopic inspections of retrieved taper connections have revealed partially overlapping surface damages such as scratches, discolorations, deformation, pitting, fretting scars, intergranular corrosion, wear and tribofilm formation at the taper interfaces in similar and mixed-alloy combinations with different surface finish and engagement lengths (Cook et al., 2013; Goldberg et al., 2002; Grupp, Weik, Bloemer, & Knaebel, 2010). The critical factors in fretting corrosion damage are different material combinations, long implantation time, apparent engagement length between head and stem taper, reduced flexural rigidity, and increased head size (Arnholt et al., 2017; Cartner, Aldinger, Li, & Collins, 2017; Di Prima et al., 2015; Goldberg et al., 2002; Goldberg, Buckley, Jacobs, & Gilbert, 1997; Kurtz et al., 2015). A multitude of retrieval studies regarding the taper connection of hip implants have been published, describing the various damaging modes (Bishop et al., 2013; Gilbert et al., 2015; Gilbert, Buckley, & Jacobs, 1993; Goldberg et al., 2002; Hall et al., 2018). Taper junctions of anatomical shoulder implants resemble those of hip implants in many ways, but they are far less studied (Day et al., 2015; Eckert, Mueller, Jaeger, Panzram, & Kretzer, 2016; Teeter, Carroll, Walch, & Athwal, 2016). While all metal implants are prone to corrosion processes in the human body, there is no qualitative evidence of corrosion occurring at the modular taper junction of TSA until today. Since the problem of MACC is well documented and is the reason for revision surgeries in total hip arthroplasty, the question arises to what extent corrosion on less weight-bearing TSA has an influence on the clinical performance. These findings are essential to develop technical solutions for the avoidance of tribocorrosion.

Although the anatomy, range of motion and load capacity between hip and shoulder arthroplasty are different, the applied materials are similar. The humeral stem is predominantly made of Co28Cr6Mo (CoCrMo) or Ti6Al4V alloy (TiAlV, ISO 5832-3, ASTM F136), whereas the humeral head can be made of CoCrMo alloy, wrought stainless steel (316L ISO 5832-1/-9) or alumina ceramic (ISO 6474). The applied CoCrMo alloys can be either cast form (ISO 5832-4, ASTM F75) or wrought form of high or low carbon content (ISO 5832-12, ASTM F1537).

The modern humeral stem designs can basically be differentiated into stemless or short stemmed fixations in the metaphysis or standard stemmed TSAs, which may be fixed cemented or cementless into the proximal humerus. In TSA the glenoid component is made of ultra-high molecular weight polyethylene and cemented in the prepared glenoid. Partial replacement of solely the humeral component by preserving the intact glenoid is known as hemiarthroplasty (HA). In comparison to the high load-bearing hip arthroplasty with measured loads

of 3 times body weight during gait and maximum loads of nearly 9 times body weight during stumbling (Bergmann, Graichen, & Rohlmann, 2004), the shoulder joint bears 1.5 times body weight during daily activities and maximum loads of 2.5 times at forward flexion (Schwachmeyer et al., 2013; Westerhoff et al., 2009).

The purpose of this study was to determine the occurring damage types in the taper junction of anatomical total shoulder and hemiarthroplasties. Particularly, we assessed the incidence rate of specific damage scores of retrieved stem and head tapers and the relation to the material combination (similar, mixed), taper surface topography and the observed failure modes. Especially, the following research questions were addressed: (a) Which damage types occur in our cohort with the corresponding incidence rate? (b) Which corrosion processes can be detected in taper junctions of TSA? (c) How are the corrosion and damage processes linked to clinical (e.g., service life), material (e.g., alloy type) and surface parameters (e.g., processing)?

2 | MATERIALS AND METHODS

2.1 | Epidemiology and explant information

A consecutive cohort of 35 retrieved anatomical shoulder endoprostheses were investigated in this study. The revision surgery of all explants was conducted at the Department of Orthopaedic Surgery at the Magdeburg University Hospital between the years 2010–2018. Institutional review board (IRB) approval for the study was provided by the local Ethical Committee of the Otto-von-Guericke University Medical School Magdeburg prior to commencement of the study (IRB No. 150/12). Additionally, informed consent for destructive tests of the implants was obtained from all patients. The mean implantation time was 3.9 ± 4.5 years (0.17–22 years) for 23 female and 12 male patients. The relevant demographic information is shown in Table 1.

The main reasons for revision surgery were secondary implant failure due to a subsequent rotator cuff deficiency or progressive glenoid erosion with an occurrence rate of 29% followed by periprosthetic

TABLE 1 Patient demographics of the retrieved anatomical shoulder implants (mean values \pm SD)

Parameter	Value
Number of patients	35
Number of retrieved TSA	8
Number of retrieved HA	27
Age (years)	69 ± 11 (41–89)
Gender	
Female	23 (65.7%)
Male	12 (34.3%)
In vivo duration (years)	3.9 ± 4.5 (0.17–22)
Side of the joint	
Left	15 (42.9%)
Right	20 (57.1%)
BMI (kg/m^2)	31.3 ± 6 (20–46)

TABLE 2 Reasons for revision surgery of the analyzed cohort

Reason for revision surgery	Total	TSA	HA	No. of previous revision surgical procedure
Secondary implant failure	10 (29%)	1 (13%)	9 (33%)	1 (30%). 2 (10%)
Periprosthetic fracture	9 (26%)	2 (25%)	7 (26%)	
Infection	6 (17%)	2 (25%)	4 (15%)	3 (17%)
Aseptic loosening	6 (17%)	3 (38%)	3 (11%)	1 (17%)
Instability	4 (11%)		4 (15%)	2 (25%) 1 (25%)
	35	8	27	8 retrievals with previous surgery

fracture with 26%, infection and aseptic loosening each with 17%. The number of previous surgical procedures at the shoulder joint before the revision surgery is presented in detail in Table 2. Manufacturers included Mathys ($n = 17$), Biomet ($n = 7$), aap ($n = 4$), Arthrex ($n = 2$), Plus Orthopedics ($n = 1$), Tornier ($n = 1$), DePuy ($n = 1$), Zimmer ($n = 1$), and Argomedical ($n = 1$). The primary articulation was metal-on-polyethylene (MoP) in 17% of cases, ceramic-on-polyethylene (CoP) in 6% of cases and 77% of our cohort where hemiarthroplasties. The majority of humeral heads had a diameter of 41 mm ($n = 6$) and 43 mm ($n = 5$) which ranged from 39 to 52 mm. Twelve out of thirty five humeral heads had an eccentric center of rotation. Regarding the bone fixation of the weight-bearing implant components, 14 were cemented one-piece stems, 11 had a cemented modular fracture stem, and 10 had an uncemented short stems. Among all humeral stems, 28 were made of TiAlV alloy and seven of CoCrMo alloy (Table 3). Inclusion criteria was the explantation of all prosthetic components and the availability of all clinical and patient related data.

2.2 | Radiographic analysis

In order to evaluate the periprosthetic bone resorption, preoperative X-ray scans were analyzed for the location and extent of radiolucent lines (RLLs) around the humeral component. Therefore, a modified Neer rating system according to Sperling et al. was used that evaluates humeral RLLs in eight radiologic zones (Neer, Watson, & Stanton, 1982; Sperling, Cofield, O'Driscoll, Torchia, & Rowland, 2000). Due to the limited number of cases, the glenoid components were not assessed.

2.3 | Taper damage

2.3.1 | Cleaning

Immediately after revision surgery, all explant components were decontaminated and cleaned using an automated disinfection program at 99°C for 10 min followed by a rinsing with demineralized water at 93°C for 5 min and 20-min drying process in the washer-disinfectors (Miele Professional, Gütersloh, Germany) of the central sterilisation department. The cleaning detergent was 10 ml/L Neodisher Mediclean forte (Dr. Weigert, Hamburg, Germany). In

special cases, further cleaning was needed to evaluate the damaged areas using warm water and soft sponges.

2.3.2 | Macroscopic damage

Joined taper junctions were disaligned in liquid nitrogen. Afterward, the components were first photographed (macro graphic workstation with AxioCam MRc 5, Carl Zeiss, Jena, Germany) and secondly inspected macroscopically using a stereo microscope (Stemi 2000 C, Carl Zeiss, Jena, Germany). A modified Goldberg score was applied which is a well-established scoring classification system to identify visual damages resulting from fretting (Goldberg et al., 2002; Higgs et al., 2013). All stem trunnions and head tapers were assessed visually according to four levels of damage from minimal, mild and moderate to severe cases with a score from 1 to 4, respectively. Two experienced researchers (N.M. and M.C.) assigned independently the scores excluding obvious damages due to the joining and disassembly process. Discrepant results were discussed to reach consensus.

2.4 | Taper topographies and geometry

Tactile surface roughness measurements of each taper sample were performed with the measuring device Form Talysurf PGI DIA Testor 7,521 (Taylor Hobson Precision, Leicester, England). According to DIN EN ISO 4288:1998, a measuring distance of 5×0.8 mm for the head taper and 5×2.5 mm for the stem tapers was specified. All samples were measured at three different locations with a radial distance of 45°. In addition, 3D topography images were obtained with a confocal microscope (μ surf expert, NanoFocus AG, Oberhausen, Germany). The measuring field of 1.57×1.57 mm was acquired with a $\times 10$ magnification objective and a vertical resolution of 20 nm.

In order to classify the different taper designs, an electronic caliper gauge (Holex 150 mm, Hoffmann SE, Munich, Germany, maximum permissible error of 30 μ m) was used to measure the minor and major diameter of the stem and head tapers as well as the taper lengths. The corresponding taper ratio was calculated by dividing the difference between these two diameters by the taper length. Moreover, the taper surfaces of five different taper designs (with $N > 2$) were scanned pointwise using a Leitz PMM 866 coordinate measuring machine (Hexagon Metrology GmbH, Wetzlar, Germany) with a LSP-X5 probe head to measure precisely the taper angle. Minor and major

TABLE 3 Data on retrieved implant components

Taper material combination	N	In vivo duration (years)	Bearing	Stem design and fixation ^a	CoCrMo head alloy type	Head diameter (mm)	Manufacturer
CoCrMo/TiAlV	17	4.4 ± 5.2 (0.3–22)	HA (n = 15)	One (n = 9)	Wrought	39 (n = 3)	Mathys (n = 7), aap (n = 4), Arthrex (n = 2), Biomet (n = 1), Tornier (n = 1), Zimmer (n = 1), plus (n = 1)
						40 (n = 1)	
			CoP (n = 2)	Modular (n = 8)	Cast	41 (n = 3)	
						42 (n = 2)	
			43 (n = 2)				
			44 (n = 3)				
			45 (n = 1)				
			46 (n = 1)				
			48 (n = 1)				
			CoCrMo/CoCrMo	7	4.3 ± 3.1 (0.6–11)	HA (n = 3)	
MoP (n = 4)	One (n = 1)	Cast					43 (n = 2)
						44 (n = 1)	
45 (n = 1)							
48 (n = 1)							
50 (n = 1)							
Ceramic/TiAlV	10	1.7 ± 1.9 (0.17–5.5)	HA (n = 8)	Modular (n = 6)	Ceramic	41 (n = 2)	Mathys (n = 10)
						CoP (n = 2)	
			43 (n = 1)				
			44 (n = 1)				
			45 (n = 1)				
			46 (n = 1)				
			47 (n = 1)				
48 (n = 1)							
316L/TiAlV	1	13	HA (n = 1)	One (n = 1)	316L	52 (n = 1)	Argomedical (n = 1)
Total	35	3.9 ± 4.5 (0.17–22)					

^aStem design and fixation are differentiated into cemented one-piece stems (one), cemented modular fracture stem (modular), and uncemented short stems (short).

diameter were determined 1 mm above and below the surface planes. Diameters at five z-levels were measured with 36 scan points and the entity of points mathematically linked via the Gauss method determined the taper angle. The device has a measurement uncertainty of 0.6 μm.

2.5 | Metallography

In order to determine the microstructure of the metallic tapers, cross sections were customized by an electrical discharge machining process (Mitsubishi MV2400S, Mitsubishi Electric, Japan). After a hot mounting process in a conductive phenol resin with carbon additive (PolyFast, Struers GmbH, Dresden, Germany), a manual grinding process was conducted with increasing grit (granulation 320–2,500) of abrasive silicon carbide paper under flowing tap water. Subsequently, a chemical mechanical polishing process with a mixture of silicon oxide and hydrogen peroxide (20%) on synthetic fiber for 10 min

generated a scratch- and deformation-free surface. Electrochemical etching was applied to visualize the microstructure. The electrolyte was ethanol with 60% perchlorid acid at a voltage of 2.5 V for 10 s.

2.6 | Scanning electron microscopy

Twenty representative components were imaged and analyzed using a scanning electron microscope (SEM) equipped with an energy dispersive X-ray spectroscopy (EDS) system (FEI Scios DualBeam, Thermo Fisher Scientific, Waltham, MA). SEM investigations were conducted using an acceleration voltage of 10–25 keV. Essential regions of interest were identified using an imaging mode at lower magnifications (×150). Taper surfaces were imaged with secondary electrons (SE) and backscattered electrons (BSE) using a Centaurus (CEN) BSE detector. Chemical analyses were performed by EDS at higher magnifications (up to ×5,000).

2.7 | Statistical analysis

All descriptive data are mean \pm standard deviation (SD). The roughness parameters among the different explants were compared using the one-way analysis of variance (ANOVA). The correlation between the incidence rates of the identified damages and defects according to the head and stem taper finish as well as of different RLL zones according to the head material was statistically evaluated with two-way ANOVA and a posthoc Fisher's least significant difference test. Level of significance (p) was set at $p < .05$ for all statistical tests. The statistical analyses were performed using Origin software (OriginLab Corporation, Northampton, MA).

3 | RESULTS

3.1 | Assessment of taper damage scores

The consecutive cohort of 35 anatomical shoulder retrievals was evaluated according to the modified Goldberg score. The graded damage scores are shown in Figure 1c. Fretting and corrosion (Score ≥ 2) were detected on 31 (89%) head tapers and 26 (74%) stem tapers with a small difference in their average damage score (2.4 ± 0.8 , 2 ± 0.8 , respectively). Head tapers exhibited more serious tribocorrosion (Score ≥ 3) with 17 cases than stem tapers with only 6, whereas severe damage (Score ≥ 4) was present on 3 heads and 2 stem tapers. Representative images of minimally and severely affected head and stem tapers are shown in Figure 1. Damage patterns have been observed in all material couplings of head and stem tapers.

3.2 | Taper topographies and geometry

For a detailed characterization of the analyzed cohort, the topography of unloaded areas of all stem and head tapers was investigated using confocal microscopy. Figure 2 shows typical examples of different surface finishes at the taper. TiAlV alloy stem tapers show either an aperiodic profile due to corundum blasting (Figure 2a) or a periodic surface profile with machining marks from the turning process (Figure 2b), whereas CoCrMo alloy stems always exhibit periodic machining marks (Figure 2c). Humeral head tapers of sintered aluminum oxide ceramic were grinded with a diamond tool, which resulted in an aperiodic taper surface profile, and heads of CoCrMo alloy (Figure 2d) were machined by a turning process and exhibit periodic machining marks (Figure 2e).

In addition, roughness parameters according to DIN EN ISO 4287 such as the arithmetic average roughness (R_a), average maximum profile height (R_z), mean line peak spacing for periodic profiles (RS_m) and core groove depth (R_k DIN EN ISO 13565-2) were measured tactilely. The mean values and standard deviations are listed in Table 4. For stem tapers the means of arithmetic average roughness R_a varied between 1.59 and 3.27 μm and the maximum profile height R_z from 8.15 to 20.01 μm . Regarding these values, there is a significant difference between turned CoCrMo or TiAlV alloy stems to TiAlV blasted taper surfaces ($p = .023$), whereas no significant differences were detected between the metals used for the stems. The peak spacing between the machining marks varied between 49.7 to 206.3 μm due to the wide range of manufacturers. The tapers of the humeral heads differed in a smaller range in all measured roughness parameters. The mean R_a values varied between 0.85 and 0.93 μm and mean R_z

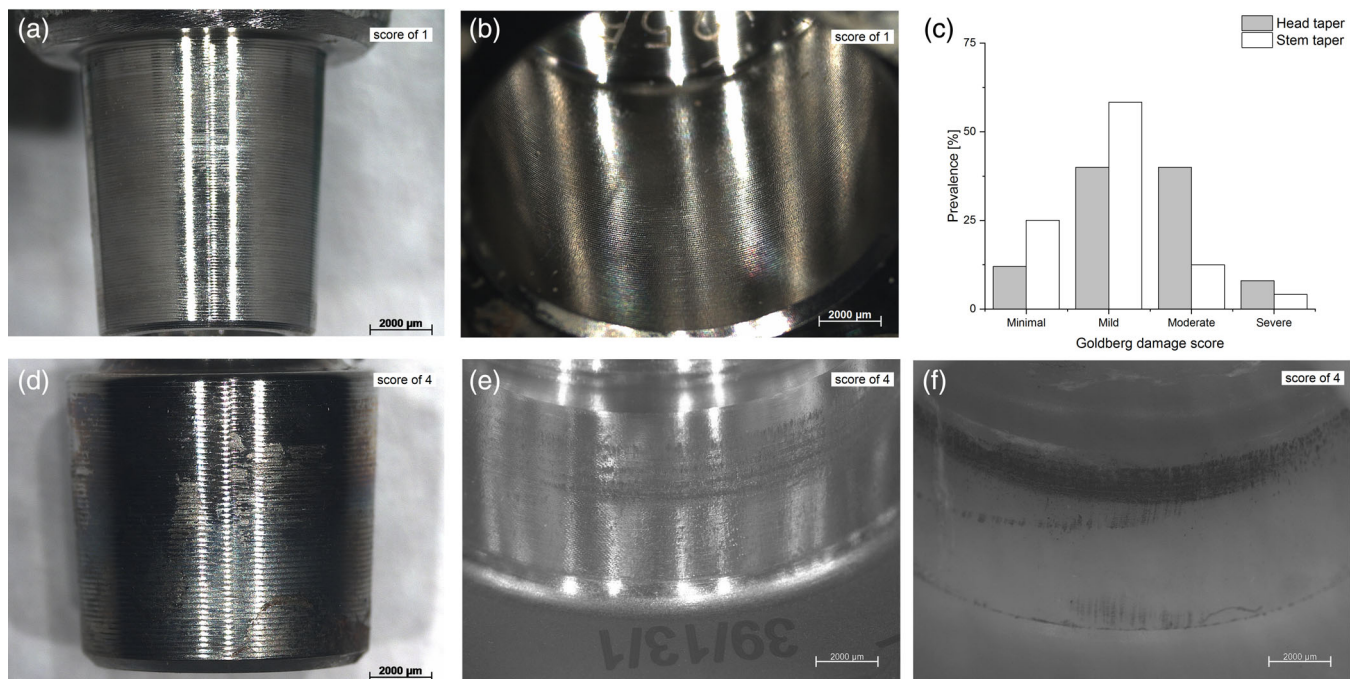


FIGURE 1 Representative images of a stem and head taper with different damage scores. Minimal taper damage (score of 1) of a (a) CoCrMo wrought alloy stem and (b) CoCrMo wrought alloy head taper and severe taper damage (score of 4) of a (d) TiAlV stem taper, (e) CoCrMo cast alloy head and (f) ceramic head taper. (c) Comparison of the incidence rate of damage scores on the assessed head and stem tapers of the retrieval cohort

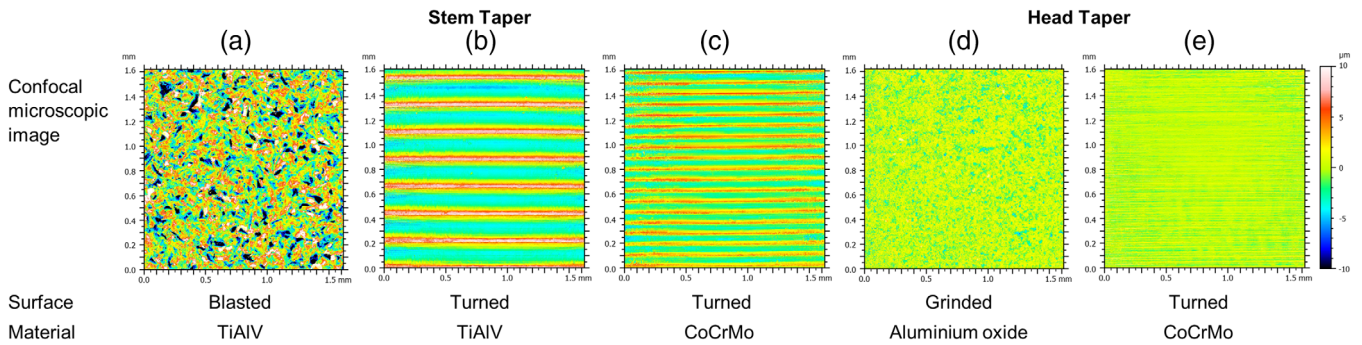


FIGURE 2 Representative confocal microscopic images of stem and head tapers of unloaded areas that show different surface finishes (corundum blasted (a), turned (b,c,e) and sintered (d)) of the commonly used materials. The tapers are oriented in proximal (top) to distal (bottom) direction

TABLE 4 Roughness parameters of all stem and head tapers according to their material and surface finish (values represent mean \pm SD)

Taper	Material	Surface	R_a (μm)	R_z (μm)	R_k (μm)	RS_m (μm)	p -value ^a
Stem taper	CoCrMo	Turned	2.03 \pm 0.11	10.48 \pm 0.74	5.23 \pm 0.57	94.25 \pm 8.61 (80.5–102.3)	$p = .02$
	TiAlV	Turned	1.59 \pm 0.08	8.15 \pm 0.67	2.96 \pm 0.54	144.15 \pm 62.06 (49.7–206.3)	
	TiAlV	Blasted	3.27 \pm 0.4	20.01 \pm 2.5	9.71 \pm 1.52		
Head taper	CoCrMo	Turned	0.93 \pm 0.2	6.86 \pm 1.5	2.80 \pm 0.61	82.69 \pm 56.92 (45.2–185.2)	
	Ceramic	Sintered	0.85 \pm 0.07	6.36 \pm 0.59	2.43 \pm 0.23		

^aA significant difference in the R_a values was observed between turned and blasted stem tapers.

between 6.36 and 6.86 μm . This indicates that the head tapers are smoother compared to the stem tapers. In comparison, the roughness parameters of the CoCrMo humeral tapers did not show significant differences to the ceramic tapers.

In addition, the geometry of the retrieved tapers was determined regarding minor and major taper diameter, taper length and taper angle. The results are summarized in Table 5 and Table S1. Stem tapers of CoCrMo alloy exhibit the smallest mean of minor taper diameter with 7.24 mm whereas TiAlV alloy stems demonstrate an increased mean of 11.04 mm for turned and 16.89 mm for blasted taper surfaces. Besides similar mean taper lengths of all stems of 8.81–10.5 mm, the range varies immensely between 8 and 16 mm. Regarding the humeral head tapers, CoCrMo alloy heads exhibit a smaller mean value for the minor diameter of 10.86 mm in comparison to 16.71 mm for ceramic heads. The taper length differs immensely between 5 and 13 mm for head tapers of CoCrMo alloy and 6.5 to 7.5 mm for ceramic heads. The multitude of taper design is reflected in the wide range of minimal and maximal minor taper diameters and lengths. Interestingly, the cohort shows a similar taper ratio for stem and head tapers with mean value of 0.101–0.109. This indicates that despite the large number of manufacturers and various technical features, similar taper angles are applied. The determined mean taper angles of five different taper designs varied for trunnions in the range from 5.67° to 5.958° and for head tapers from 5.665° to 6.004° (Table S1). These values show an approximately good agreement with the FDA recommendation for hip tapers of 5.6167°–5.7083° and

other publications (Gilbert et al., 1993; Grupp et al., 2010; Lundberg, Ha, Hall, Urban, & Levine, 2015; Rehmer, Bishop, & Morlock, 2012). The angles vary distinctively between the manufacturers, whereas pairing of components from the same taper design exhibit mostly congruent angles. An increased taper clearance with 0.075°–0.092° between head and stem taper angle is observed for corundum blasted pairings.

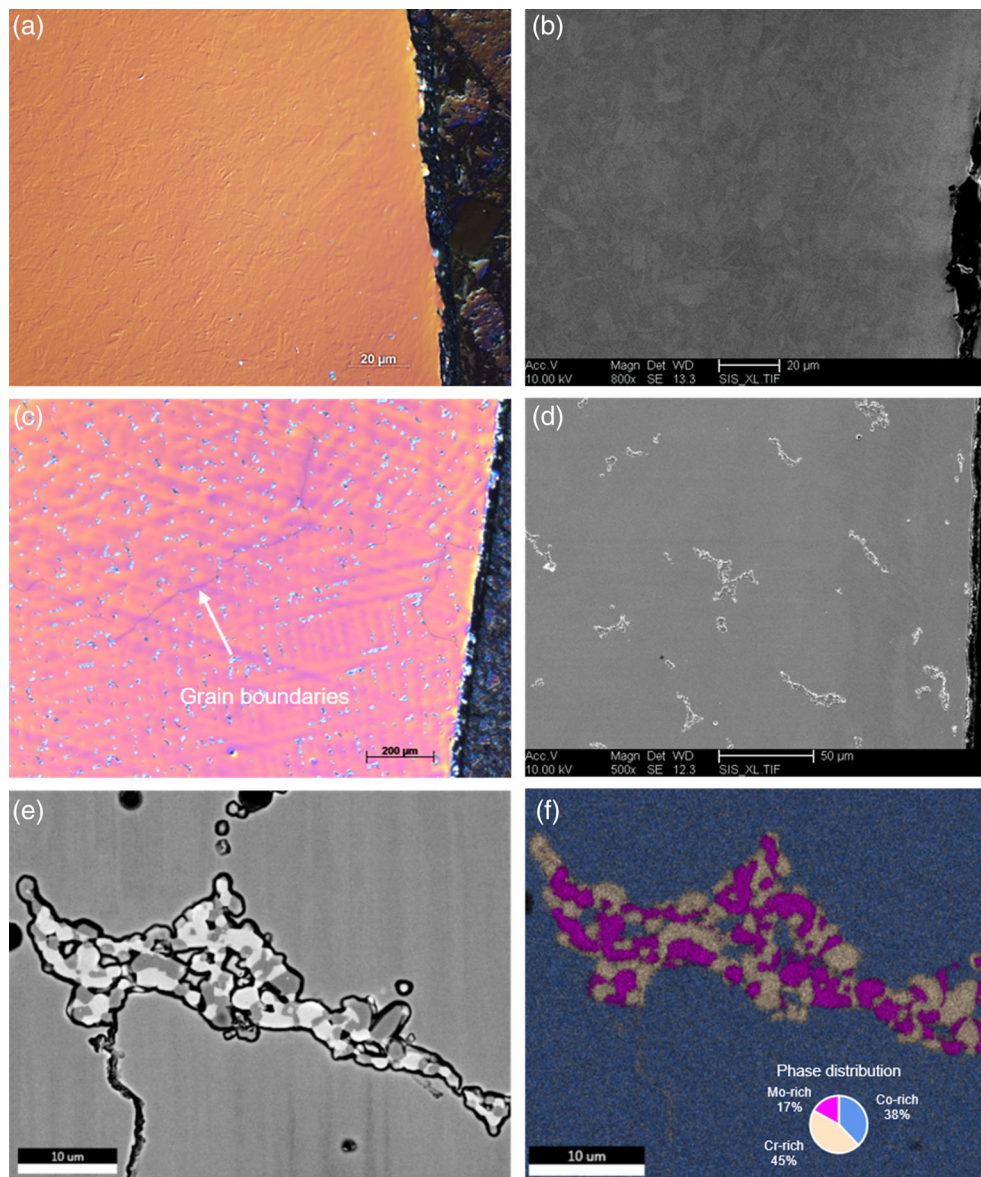
3.3 | CoCrMo microstructure

The metallographic sections of the CoCrMo humeral stem and head tapers were imaged with optical and scanning electron microscopy and are shown in Figure 3. Both cast and wrought alloy exhibited their specific characteristic alloy microstructure.

The investigated CoCrMo wrought alloy is fine-grained with grain sizes between 3 and 5 μm and shows an enhanced chemical homogeneity (Figure 3a,b). In contrast, CoCrMo cast alloys exhibit a typical dendritic microstructure and grain sizes in the scale of ~800 μm (Figure 3c,d). Moreover, an irregularly distributed secondary phase is visible which can be attributed to different characteristic hard phases (Jenko et al., 2018; Karpuschewski, Pieper, Krause, & Döring, 2013). Backscattered electron contrast images show them with grey scale differences that are associated with variances in the chemical composition (Figure 3e). This was verified in the EDS mapping that shows phases of increased chromium and molybdenum concentrations in comparison to the CoCrMo primary

TABLE 5 Geometric parameters for stem and head tapers according to their material and surface finish (values represent mean \pm SD and the range from minimum to maximum)

Taper	Material	Surface	N	Minor taper diameter (mm)	Taper length (mm)	Taper ratio
Stem taper	CoCrMo	Turned	7	7.24 \pm 0.39 (7–8)	10.5 \pm 2.76 (9–16)	0.109 \pm 0.007
	TiAlV	Turned	11	11.04 \pm 2.24 (7.4–15)	10.35 \pm 1.88 (8–16)	0.101 \pm 0.031
	TiAlV	Blasted	17	16.89 \pm 2.35 (16–23)	8.81 \pm 0.93 (8–11)	0.104 \pm 0.009
Head taper	CoCrMo	Turned	24	10.86 \pm 3.91 (7–15)	9.72 \pm 2.67 (6–13)	0.105 \pm 0.025
	Ceramic	Grinded	10	16.71 \pm 0.06 (15.9–22.8)	6.5 \pm 0.02 (6.5–7.5)	0.101 \pm 0.006

**FIGURE 3** Optical microscopic images with polarizing filter (a,c) and SEM images of metallographic cross sections of different CoCrMo alloy heads. (a,b) Humeral head of CoCrMo wrought alloy (ASTM F1537, ISO 5832-12) exhibits small grain sizes in the order of 3–5 μ m and a homogeneous chemical composition. (c,d) Dendritic microstructure of a head of CoCrMo cast alloy (ASTM F75, ISO 5832-4) showing a secondary phase also along the grain boundaries. It is characterized by large grains (>800 μ m). (e) Backscattered electron contrast image of (c) with a higher magnification of the secondary phase and (f) the corresponding EDS mapping that demonstrates a heterogeneous chemical composition with deviating Cr-, Mo-, and Co-rich phases. All images are oriented from proximal (top) to distal (bottom) direction along the head taper counter

phase (Figure 3f). The process of chemical segregation occurs as the casting solidifies and results in characteristic carbon forming chromium carbides (Herrera et al., 2005; Weeton & Signorelli, 1954). Out of 24 humeral CoCrMo alloy heads, 12 were cast alloy

by three manufacturers and 12 exhibited wrought alloy produced by five manufacturers. Two manufacturers used CoCrMo alloy stems of which six were CoCrMo wrought alloy and one CoCrMo cast alloy.

3.4 | Taper damage features and types

The analyzed retrieval cohort illustrated local defect features that correspond to different basic wear mechanisms defined in the standard DIN 50320:1979-12 and refined submechanisms (Dienwiebel, 2018; Stemmer & Fischer, 2018). In order to define countermeasures that prevent the distinguished damages, an understanding of the multifactorial interdependencies on macro-, micro-, and nanoscale of the tribological taper system is of uppermost importance.

The analyzed taper surfaces revealed damages such as plastic deformation, material transfer, film and deposit formation, particle induced microploughing, mechanically and electrochemically dominated fretting, and residues of moving cells. The incidence of the specified defect types differs between the surface material combination and surface finish for stem and head tapers. In the following, characteristics of each damage type will be illustrated and defined in detail.

The functionality of the cone taper connection is based on elastic and *plastic deformation* of the machining mark peaks that are caused

by the joining, in vivo loading and disassembly processes. The plastic flattening process is present on all stems independent of the surface finish or alloy composition (Figure 4a,b). The flattened machining peaks deformed approximately by 20% of the maximum peak height as illustrates in the tactile measured height profile of an exemplary TiAlV alloy stem (Figure 4c). In addition, some deformed peaks were covered with linear grooves in axial direction (Figure 4a) that demonstrate abrasive microploughing. This overlapping mechanism of plastic deformed machining marks with deep linear grooves was mainly present on tapers with a mixed CoCrMo/TiAlV alloy combination.

Besides the plastic deformation, there is evidence of *adhesive material transfer* and related cohesive material defects from the stem to the head taper and vice versa. Different grey-scales in the backscattered electron contrast images (CEN detector) distinguish the disparate alloy distribution. Figure 4d illustrates a case in which the CoCrMo alloy head taper is covered by adhering residues of the TiAlV alloy stem (Figure 4d) and corresponding surface breakouts on the TiAlV alloy stem (Figure 4f). Besides titanium, the adhering material

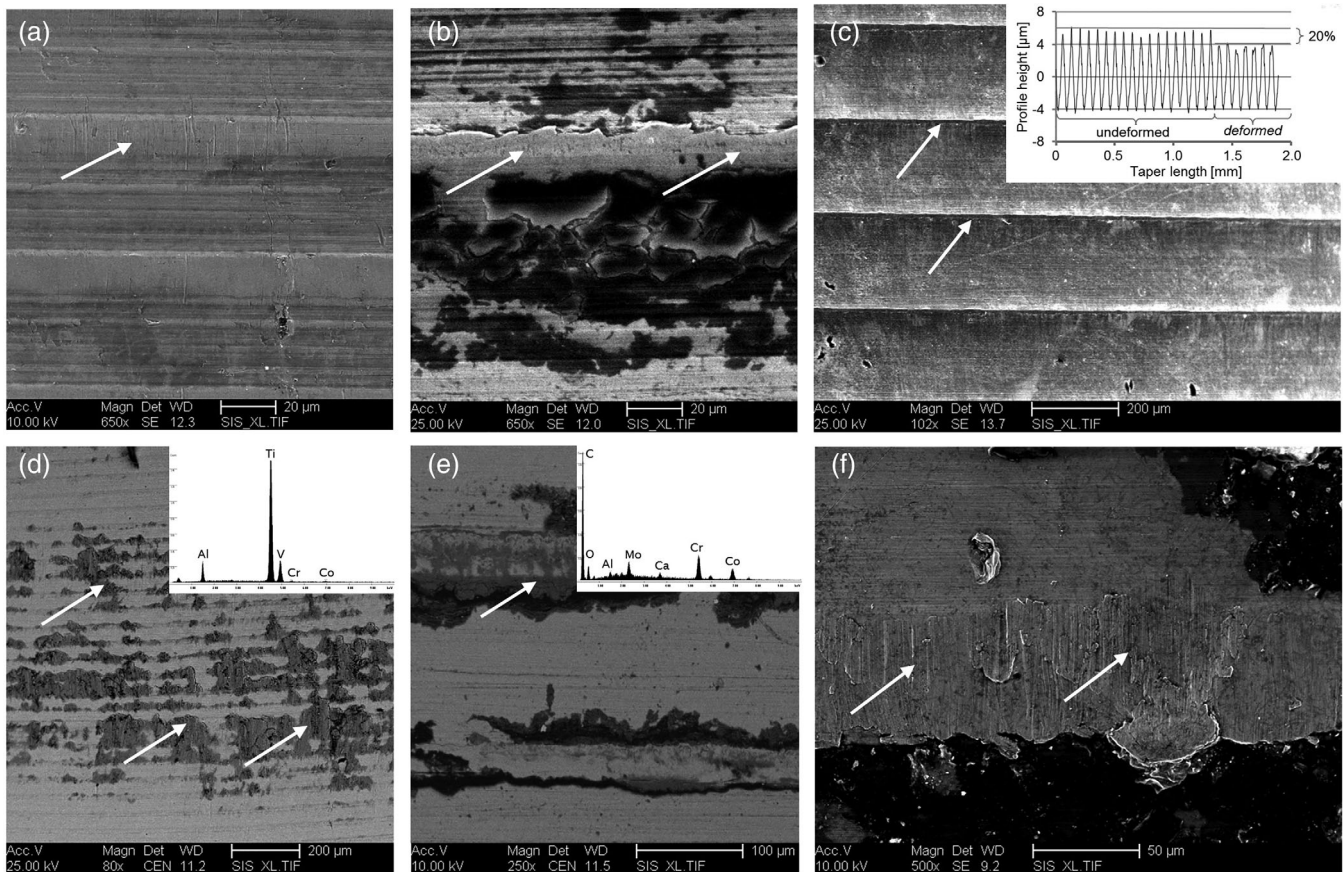


FIGURE 4 Scanning electron microscope (SEM) images that demonstrate plastically deformed machining marks and backscattered electron contrast images (CEN detector) with adhering material residues of different taper surfaces. (a) Widespread compressed bands characterize deformed machining peaks on a CoCrMo alloy head aligned with a TiAlV alloy stem. (b) Flattened machining marks with deformed edges on a CoCrMo alloy stem coupled with a CoCrMo alloy humeral head. (c) Roughness profile section of a tactile measurement on a TiAlV alloy stem showing the transition from an unloaded to a plastically deformed section. The maximum peak height is deformed by ~20%. (d) CoCrMo alloy head taper with extensive TiAlV alloy flakes (dark areas) that have been transferred from the stem taper. The EDS spectrum verifies the elements of a TiAlV alloy. (e) TiAlV alloy stem taper of a CoCrMo/TiAlV couple with accumulated organic residues as well as chromium and molybdenum oxides at the flattened machining marks. Besides the occurrence of adhesion there is an accumulation of corrosion products observable. (f) SEM image of characteristic material breakouts on a TiAlV alloy stem taper

did contain the alloying elements aluminum and vanadium indicating TiAlV alloy in the EDS spectrum. Moreover, some cases of TiAlV stem tapers exhibited an adhering mixture of organic as well as chromium and molybdenum oxides from the aligning head taper (Figure 4e). Material transfer was more pronounced on mixed compared to similar material couplings. Accordingly, 50% of stems and 40% of heads in CoCrMo/CoCrMo couples exhibited material transfer in comparison to mixed combinations with 87% and 94% for CoCrMo/TiAlV combinations. All mixed couplings that involved a ceramic head revealed large areas affected of adhesion with TiAlV alloy flakes to the head tapers (Figure 1f).

Besides the adhesive material transfer, there are examples of thick *deposits*, *tribological film formation*, and *organic residues* in the troughs of the machining marks on almost all stem and head tapers. In most cases, the EDS spectra revealed strong carbon, oxygen as well as molybdenum and chromium peaks (Figure 5a). Some cases were found with a peak of phosphorus and chromium oxide indicating the occurrence of chrome phosphates (Figure 5b,c). This carbonaceous adhesive layer was present on all material combinations as

well as on the stem and head tapers. Some carbonaceous deposits were flake-shaped or even showed cracks, but all accumulated in the unloaded machining ridges.

Another observable phenomenon was the occurrence of separate organic residues that resembled cell-like structure such as macrophages regarding size and morphology. These visually resembling *adhering cells* were detected on CoCrMo alloy head tapers as well as on TiAlV alloy stems (Figure 5e,f). Their presence was more pronounced in distal taper regions outside the clamping area. Higher magnifications did not show any defect marks that may be associated with them.

Particle-induced *microploughing* was identified as a separate damage type that mainly occurred on CoCrMo alloy head tapers in combination with corundum blasted stem tapers (Figure 6). The particles adhered to the aligned counter body and produced abrasive scratches in the CoCrMo head taper (Figure 6d). EDS spectra of different spot scans verified the presence of corundum particles at the top of the scratch marks.

Damage marks characteristic for *fretting* were observed on both taper surfaces of CoCrMo and TiAlV alloy. The observed fretting

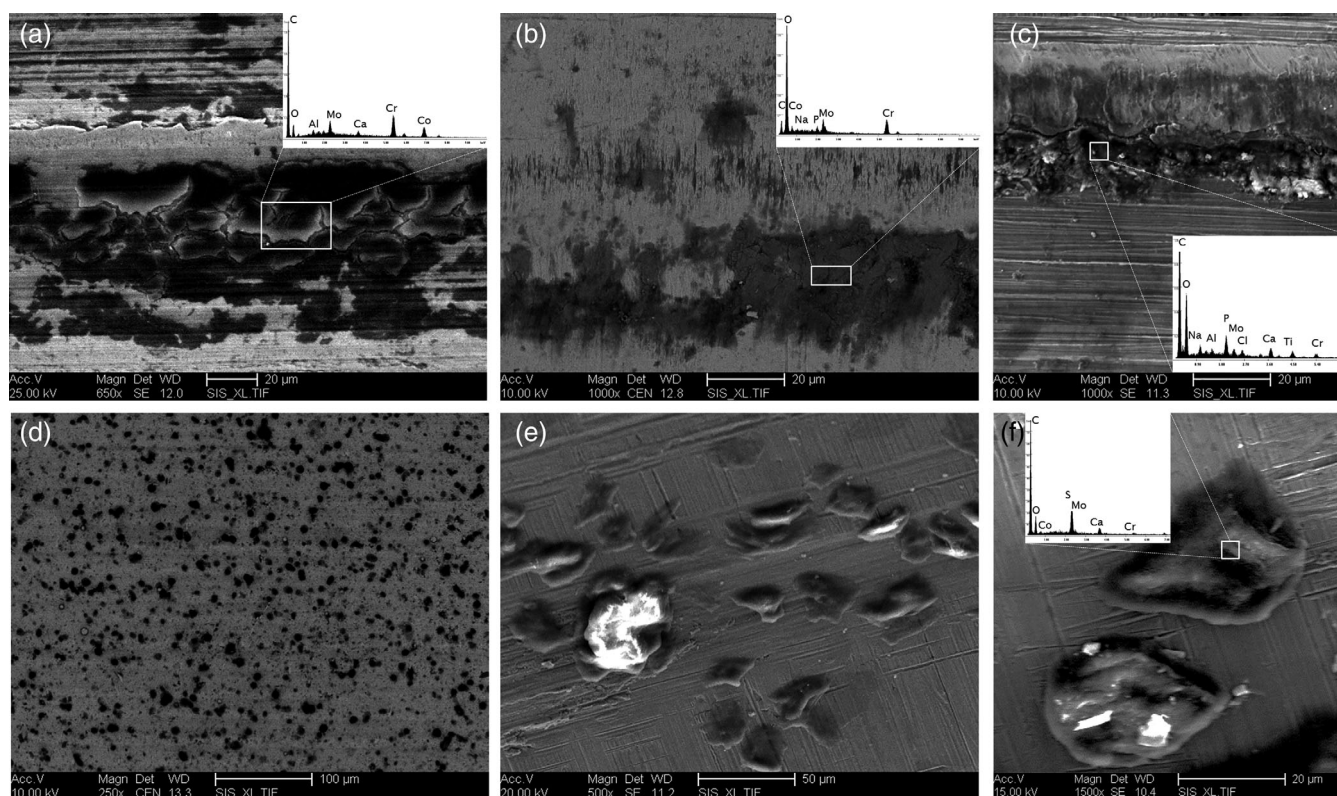


FIGURE 5 Scanning electron microscope (SEM) images of adhering tribological films, deposits and cell-shaped residues that resemble macrophages. The white frames indicate the area of the depicted energy dispersive X-ray spectroscopy (EDS) spectrum (a) SEM image of a CoCrMo/CoCrMo coupled stem taper with accumulated deposits within the machining troughs. The EDS spectrum shows high peaks of carbon, molybdenum and chromium and a lower peak of cobalt. (b) CoCrMo stem taper with a tribological layer that consists of a mixture of carbon, molybdenum, chromium, and phosphorus. (c) CoCrMo/TiAlV coupled stem taper with accumulated oxide deposits. EDS spectrum shows the occurrence of chromium and molybdenum oxide as well as some low signals of the TiAlV alloy. (d) Round shaped remnant on a CoCrMo alloy head taper that was combined with a TiAlV stem. (e) Cell-like adhesive residues on a TiAlV taper adapter in an area outside the clamping range. The adapter was coupled with a CoCrMo humeral head. (f) CoCrMo alloy head taper that was aligned with a TiAlV alloy stem shows adhering cell-shaped residues

damages were either mechanically or electrochemically dominated. Mechanically induced fretting was observed as fine, parallel arranged scratches next to flattened machining marks in axial orientation to the taper axis (Figure 7a–c,f). Typical features for fretting corrosion (Figure 7d,e) are etching patterns of elongated pits close to remnants of load-bearing deformed machining marks. Mechanical as well as electrochemical fretting occurred separately or combined. The incidence for fretting on head tapers is slightly elevated in mixed CoCrMo/TiAlV couples than in similar CoCrMo/CoCrMo couples with 31 and 20%, respectively. This difference is also present in the corresponding stem tapers with incidence rates of 20% for mixed and 17% for similar taper combinations. Moreover, mechanically dominated fretting was more dominant on CoCrMo wrought alloy and electrochemical fretting with etching marks only appeared on CoCrMo cast alloy.

The incidence rates for the identified damage modes present in our cohort of anatomical shoulder tapers are summarized in Figure 8a. The most frequently observed damage modes are plastic deformation, material transfer and the formation of tribofilms and deposits with an incidence rate of more than 70% in our cohort. Their occurrence was independent of the material combination and taper surface finish. They originate from the alignment and in vivo loading

processes. The existence of cell-shaped residues was only observed on turned stem tapers and their corresponding head tapers. These filigrade adhesion remains were not detected on the strongly fissured stem tapers with a blasted surface finish, but their existence cannot be ruled out. The occurrence of particle-induced microploughing was significantly increased for corundum blasted stem tapers in comparison to turned tapers ($p = .0166$). Consequently 89% of blasted stems and 71% of the corresponding head tapers showed evidence of microploughing damage. Regarding the defects that can be clearly attributed to fretting and fretting corrosion, turned taper couples showed an increased incidence rate of 35% for stem and 47% for head tapers in contrast to blasted taper couples with 6% and 14%, respectively. Due to the overlapping mechanisms, it is very likely that the corundum layer hinders the complete detection of fretting damage.

The main question was to determine whether a correlation exists between the assessed taper damage to the clinical data. Therefore, RLLs on preoperative radiographic images were assessed according to Sperling et al. (2000). They revealed that bone resorption occurs with an incidence rate of 62% in all our included patients (Figure S1). The results in Figure 8b demonstrate that RLLs are predominant in the proximal zones (1, 7, and 8) of the humerus independently to the

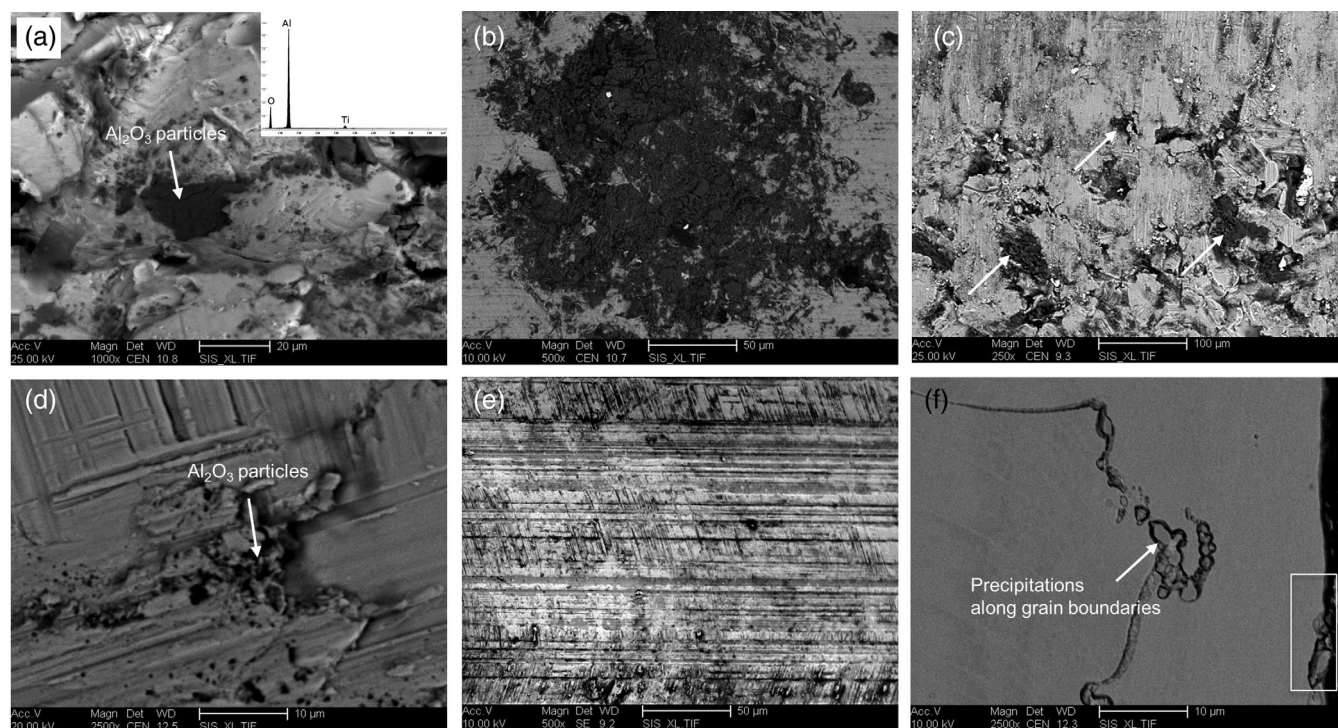


FIGURE 6 Scanning electron microscope (SEM) images of particle-induced microploughing. (a) Backscattered electron contrast image of a TiAlV/CoCrMo combined stem taper with evidence of corundum particles embedded at the surface of the clamping area. (b) TiAlV alloy taper adapter with a large area of corundum grains pressed in the taper surface. (c) TiAlV stem taper with a plastically deformed clamping area. Backscattered electron contrast displayed embedded corundum particles and their scratches. (d) CoCrMo head taper showing adhering particles that generate scratches. EDS spectra identified the dark spots as increased aluminum and oxygen peaks. (e) SEM image of (D) with a lower magnification that shows extensive scratches in all flattened machining marks due to a corundum blasted counter surface. (f) Cross section of a CoCrMo cast alloy head taper that was aligned with a corundum blasted TiAlV stem taper. Residues of corundum particles are pressed into the head taper surface (white frame)

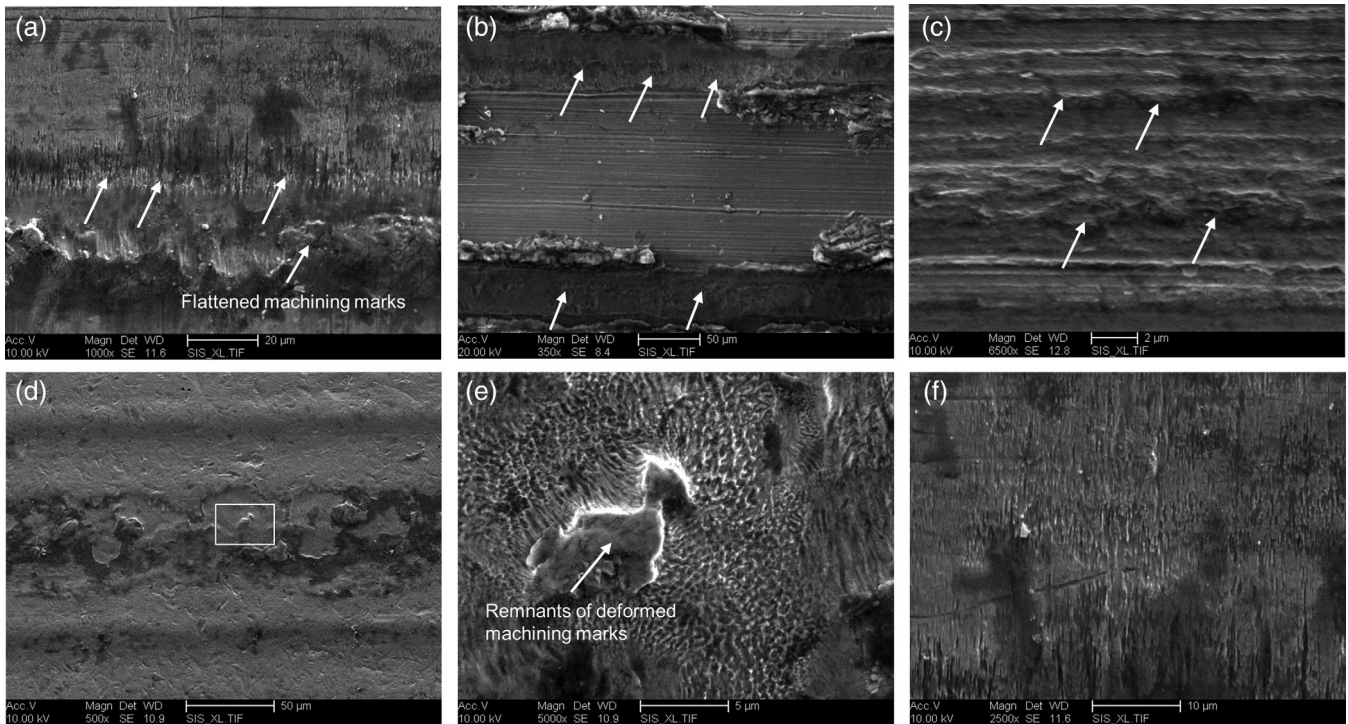


FIGURE 7 Damage features indicative for mechanically dominated fretting and fretting corrosion. (a) CoCrMo wrought alloy head taper of a CoCrMo/CoCrMo combination with characteristic fretting marks in axial orientation to the taper axis (white arrows) adjacent to the flattened machining ridge. (b) SEM image of a TiAlIV stem taper that exhibits elongated fretting pits at the edge of the deformed machining marks that are indicated by white arrows. The TiAlIV stem was aligned with a CoCrMo head taper. (c) TiAlIV stem taper with disrupted machining marks (white arrows) and evidence of mechanical fretting. (d) SEM image of a CoCrMo cast alloy head taper that illustrates a horizontal area of electrochemically dominated fretting marks. (e) A higher magnification of (d) white frame) displays the presence of strong etching patterns as well as elongated pits that are typical for corrosive damage. In the middle of the image are remnants of the deformed machining peaks. (f) Corrosion pattern on a CoCrMo head taper that evidences planar metal degradation with axial scratches. All SEM images show the tapers oriented from proximal to distal direction

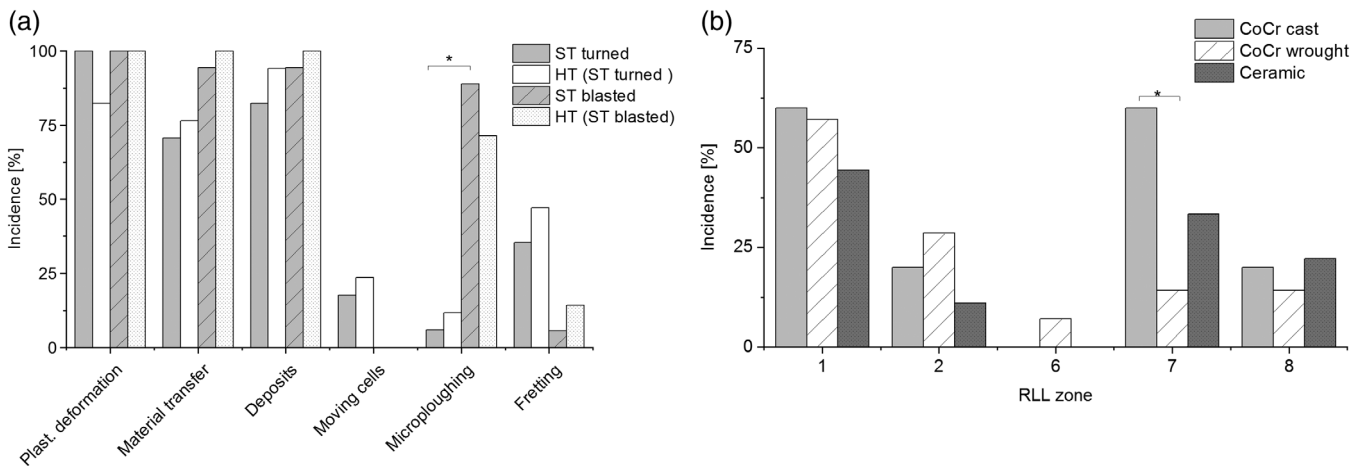


FIGURE 8 (a) Incidence rates of the identified damages and defects on stem tapers (ST) and head tapers (HT) according to the stem taper finish. The occurrence of microploughing shows a significant difference ($p = .0166$) between turned and blasted stems. (b) Results of the assessment of radiolucent lines (RLLs) in the humeral zones analyzed according to the modified Neer classification for different head materials. CoCrMo cast alloys show a significantly increased incidence for a RLL in the medial Zone 7 of the proximal humerus ($p = .0263$)

stem/head material combination or taper finish. These zones indicate a relationship to the taper junction of the implant. In addition, there is a significant difference ($p = .0263$) in the occurrence of an

RLL in the proximal area of the medial zone 7 for CoCrMo cast alloy heads with an incidence rate of 60% in comparison to all CoCrMo wrought alloy (14%) or ceramic (33%) heads of our cohort.

4 | DISCUSSION

The aim of this study was to investigate the occurring damage mechanisms in modular taper junction of contemporary anatomical shoulder endoprostheses. Therefore, a cohort of 35 explanted anatomical shoulder prosthesis was assessed for macroscopic corrosion using the modified Goldberg score (Goldberg et al., 2002; Higgs et al., 2013). We found that 89% of all investigated shoulder explants exhibited signs of macroscopic damage patterns. This is in line with publications showing similar damage scores on shoulder taper connections (Day et al., 2015; Eckert et al., 2016; Teeter et al., 2016).

In addition, taper topographies were characterized by tactile measurements and confocal microscopy. Our results reveal a manufacturer-dependent diversity of taper designs and surface finishes of either periodic machining marks or aperiodic profiles due to corundum blasting or grinding with different processing parameters. In contrast to manufacturers of hip taper junctions that follow principally the 12/14 taper diameter recommendation despite a missing taper standardization, our study shows broad variations of modular connections in anatomical shoulder prostheses, such as 7/8 or 23/24 diameter ratio, but similar taper angles to hip arthroplasty (Mueller, Braun, Schroeder, Sonntag, & Kretzer, 2017). The surface finish and taper clearance determine the engagement length, the area of contact and consequently the asperity-based interactions between the clamping surfaces that influence the taper strength. Due to a missing standard for shoulder tapers, the effect of the different taper designs on the asperity contact and stress distribution at the taper interface need further analysis. Other publications investigating hip junctions showed that the taper surface influences the damage progression and should therefore be designed with higher profile heights (Lundberg et al., 2015; Panagiotidou et al., 2013; Pourzal et al., 2016).

While the modified Goldberg score indicates only macroscopic damage features, higher resolutions applying SEM are required to identify and differentiate the specific damage mode. Using SEM, we identified various overlapping damage types in our cohort. Some damage features were similar to those found at taper junctions in hip arthroplasty. Especially plastic deformation, material transfer, tribological films, cell-like residues and corrosion damages have been detected (Gilbert et al., 1993; Gilbert, Sivan, et al., 2015; Lundberg et al., 2015). Other damage modes, such as imprinting and column damage (Hall et al., 2018), were not observed in our retrieval cohort of shoulder implants.

In 70% of our retrieved explants, the most frequent taper damages included signs of plastic deformation, material transfer, deposits and tribological film formation. They have been detected in all tested material combinations and surface finishing independent of the time of implantation. Different studies also observed similar damage modes in head-neck junctions of total hip arthroplasty (Bishop et al., 2013; Hall et al., 2018). These similarities indicate that the observed damage patterns might evolve from contact mechanics during in vivo loading as well as the implant assembly and detachment processes. Furthermore, they are indicators of contact stability and the occurrence of

micromotion at the head taper junction (Rehmer et al., 2012). A special damage type that we only detected on shoulder explants was abrasive particle induced microploughing, which was predominant for corundum blasted TiAlV alloy stem tapers leading to macroscopic material loss due to third-body wear. This damage mode has yet not been described before for any other orthopedic taper junction. The reason may be that only a few manufacturers apply corundum blasting for hip tapers.

Adhering cell-like residues occurred on different taper surfaces predominantly outside of the clamping area in distal regions. These have also been observed on hip explants (Gilbert, Sivan, et al., 2015; Hall et al., 2018). The literature regarding the influence of these cell-like structures on corrosion damaging patterns is diverse. Some studies link osteoclasts and inflammatory cells to specific material loss (Cadosch et al., 2010; Cadosch, Chan, Gautschi, Simmen, & Filgueira, 2009; Di Laura et al., 2017; Gilbert, Mali, & Sivan, 2015; Lin & Bumgardner, 2004), but the in vivo observed corrosion damage has yet not been reproduced in laboratory studies (Liu & Chen, 2018). Our data indicate that the detected cell-like structures might not influence the degradation of the underlying biomaterials, as we did not observe any surrounding defects such as etching trails.

We show that material degradation due to MACC also occurs on shoulder implants by providing the first qualitative proof of mechanically as well as electrochemically dominated fretting. SEM images demonstrate axial fretting scratches and etching patterns in the material combinations CoCrMo/CoCrMo and CoCrMo/TiAlV. Characteristic fretting damage was detected on 16% of all analyzed stem and 19% of head tapers. Similar tribocorrosion patterns have been described in taper junctions of hip prostheses in different retrieval studies (Gilbert et al., 1993; Hall et al., 2018; Kurtz et al., 2013). The incidence rates of 14–35% for corrosion damage in retrieved hip arthroplasties are in line with our observations on head and stem tapers of our shoulder cohort. This finding indicates that in vivo corrosion processes are little affected by the different designs and weight-bearing stresses on shoulder and hip arthroplasties. The observed tribocorrosion damage in the investigated shoulder explants was mainly present at the edges of deformed machining marks indicating that extreme environmental conditions, such as hypoxia or low pH values, must have been present in the forming micro-crevices.

Remarkably, mainly CoCrMo cast alloy showed a higher susceptibility to electrochemically dominated fretting with an incidence rate of about 40%, whereas tapers of CoCrMo wrought alloy exhibited mechanical fretting marks. This might also be influenced by the taper design, for example, taper angle and clearance, present in our retrievals. The observed increase in corrosion susceptibility of CoCrMo cast alloy in comparison to CoCrMo wrought alloy in our cohort could be explained by the increased formation of chromium carbides that produce narrow zones of chromium depletion and consequently restrain the formation of a stable passive layer but enforces corrosion processes, which has been shown in different experimental studies (Devine, 1976; Pourzal et al., 2017). Nevertheless, it is not known yet whether mechanically and electrochemically fretting processes overlap simultaneously or consecutively.

In addition, we found a significant increase in the occurrence of RLLs in the proximal humeral zone for CoCrMo cast alloy heads. Whether this phenomenon is directly linked to the corrosion process in the taper junction remains to be analyzed. RLLs are an indicator for bone loss, most likely by osteonecrotic processes (Boileau et al., 2015). Several studies link an increased heavy metal ion concentration to adverse biological reactions in periprosthetic tissue, system effects (Drynda et al., 2018; Hallab et al., 2004; Khair, Nam, DiCarlo, & Su, 2013) as well as an induction of osteonecrosis (Andrews, Shah, Wilkinson, & Gartland, 2011; Klutzny et al., 2019). Therefore, our findings might indicate a link between the increased corrosion susceptibility of CoCrMo cast alloy with the significant occurrence of a RLL near the taper junction. Similar processes have been described for total hip arthroplasty, where femoral RLLs have been linked to osteolysis and instability at the cone/taper interface (Meyer et al., 2012).

There are some limitations regarding this retrieval study. One limitation of this study is the retrieval cohort, which on the one hand is restricted in numbers and on the other hand comprises different implant manufacturers with various design features and a large diversity of patients. It reflects the retrieved implants at our orthopedic clinic, which is a tertiary referral center, receiving large numbers of patients with complicated revision cases. Therefore, the detected damage phenomena and identified incidence rates are restricted to the analyzed retrieval cohort of 35 cases. Moreover, the cohort comprises 12 different taper designs with a limited number of explants that were not sufficient for a statistic evaluation regarding the geometric influence on taper damage. In addition, the explants exhibit plastic deformation and surface damages that result from the mechanical joining, loading, and disjoining process. Thus, future studies should evaluate the appropriate taper design and surface structure for an ideal taper strength of anatomical shoulder prosthesis considering all relevant factors including the impact force, implant positioning and cyclic in vivo loading.

Nevertheless, this is the most comprehensive study on the damage types of contemporary taper junctions of anatomical shoulder arthroplasties representing the first qualitative evidence of corrosion damage. Critical risk factors contributing to taper damage, wear and corrosion were identified that are relevant for the development of countermeasures aiming at improved clinical performances of shoulder implants. Based on the results of this retrieval study, CoCrMo cast alloy should be excluded for articulating shoulder components due to their disadvantageous electrochemical properties. Moreover, corundum blasting on modular taper junctions should be avoided for use in TSA to minimize wear, MACC and other taper damages. In conclusion, the formation of crevices within the taper junction due to plastic deformation of machining marks or taper tilting should be limited.

ACKNOWLEDGEMENTS

The authors would like to thank Anja Schröder, Carolin Schneider, Mandy Könecke, and Michael Reppin for their excellent technical assistance and valuable support. This work was in part conducted

within the context of the International Graduate School MEMoRIAL at Otto von Guericke University (OVGU) Magdeburg, Germany, kindly supported by the European Structural and Investment Funds (ESF) under the program "Sachsen-Anhalt WISSENSCHAFT Internationalisierung"(project no. ZS/2016/08/80646).

CONFLICT OF INTEREST

Professor Christoph H. Lohmann is a paid consultant for the following companies Waldemar Link GmbH & Co. KG, Mathys Medical GmbH and ImplanTec GmbH and has royalties from ImplanTec GmbH. The authors confirm that there has been no significant financial support for this work that could have influenced its outcome.

AUTHOR CONTRIBUTIONS

M.C. performed all preparations and investigations, drafted the manuscript; N.M. provided the clinical data, helped with interpretation of data, and drafted the clinical part of the manuscript; K.H. helped with the SEM technique and interpretation of data; A.B. performed the revision surgeries and helped with the discussion and interpretation of data; J.D. helped with interpretation of data; C.H.L. supervised the interpretation of clinical data and writing of the manuscript, T.H. supervised the material corrosion data and drafted the manuscript, J.B. designed the study and helped writing the manuscript and interpreting the data.

REFERENCES

- Andrews, R. E., Shah, K. M., Wilkinson, J. M., & Gartland, A. (2011). Effects of cobalt and chromium ions at clinically equivalent concentrations after metal-on-metal hip replacement on human osteoblasts and osteoclasts: Implications for skeletal health. *Bone*, *49*, 717–723.
- Arnholdt, C. M., MacDonald, D. W., Underwood, R. J., Guyer, E. P., Rimnac, C. M., Kurtz, S. M., ... Kraay, M. J. (2017). Do stem taper micro-grooves influence taper corrosion in total hip arthroplasty? A matched cohort retrieval study. *The Journal of Arthroplasty*, *32*, 1363–1373.
- Bergmann, G., Graichen, F., & Rohlmann, A. (2004). Hip joint contact forces during stumbling. *Langenbeck's Archives of Surgery*, *389*, 53–59.
- Bishop, N., Witt, F., Pourzal, R., Fischer, A., Rüttschi, M., Michel, M., & Morlock, M. (2013). Wear patterns of taper connections in retrieved large diameter metal-on-metal bearings. *Journal of Orthopaedic Research*, *31*, 1116–1122.
- Boileau, P., Moineau, G., Morin-Salvo, N., Avidor, C., Godenèche, A., Lévine, C., ... Walch, G. (2015). Metal-backed glenoid implant with polyethylene insert is not a viable long-term therapeutic option. *Journal of Shoulder and Elbow Surgery*, *24*, 1534–1543.
- Cadosch, D., Al-Mushaiqri, M. S., Gautschi, O. P., Meagher, J., Simmen, H.-P., & Filgueira, L. (2010). Biocorrosion and uptake of titanium by human osteoclasts. *Journal of Biomedical Materials Research. Part A*, *95*, 1004–1010.
- Cadosch, D., Chan, E., Gautschi, O. P., Simmen, H.-P., & Filgueira, L. (2009). Bio-corrosion of stainless steel by osteoclasts—in vitro evidence. *Journal of Orthopaedic Research*, *27*, 841–846.
- Cartner, J., Aldinger, P., Li, C., & Collins, D. (2017). Characterization of femoral head taper corrosion features using a 22-year retrieval database. *HSS Journal*, *13*, 35–41.
- Cook, R. B., Bolland, B. J. R. F., Wharton, J. A., Tilley, S., Latham, J. M., & Wood, R. J. K. (2013). Pseudotumour formation due to tribocorrosion

- at the taper interface of large diameter metal on polymer modular total hip replacements. *The Journal of Arthroplasty*, 28, 1430–1436.
- Day, J., MacDonald, D., Abboud, J., Williams, G., Rinnac, C., Kraay, M., McCloskey, R.C., Arnholt, C. M., & Kurtz, S.M. (2015). Mechanically assisted crevice corrosion damage in shoulder arthroplasty is comparable to hip arthroplasty. In A. S. Greenwald, S. M. Kurtz, J. E. Lemons, & W. M. Mihalko (Eds.), *Modularity and tapers in total joint replacement devices*. ASTM international: West Conshohocken, PA, (pp. 181–191).
- Deore, V. T., Griffiths, E., & Monga, P. (2018). Shoulder arthroplasty—Past, present and future. *Journal of Arthroscopy and Joint Surgery*, 5, 3–8.
- Devine, T. M. (1976). The comparative crevice corrosion resistance of Co-Cr Base surgical implant alloys. *Journal of the Electrochemical Society*, 123, 1433.
- Di Laura, A., Hothi, H. S., Meswania, J. M., Whittaker, R. K., de Villiers, D., Zustin, J., Blunn, G. W., Skinner, J. A., & Hart, A. J. (2017). Clinical relevance of corrosion patterns attributed to inflammatory cell-induced corrosion: A retrieval study. *Journal of Biomedical Materials Research. Part B, Applied Biomaterials*, 105, 155–164.
- Di Prima, M. A., Vesnovsky, O., Kovacs, P., Hopper, R. H., Ho, H., Engh, C. A., & Topoleski, L. D. T. (2015). Comparison of visual assessment techniques for Wear and corrosion in modular hip replacement systems. In A. S. Greenwald, S. M. Kurtz, J. E. Lemons, & W. M. Mihalko (Eds.), *Modularity and tapers IN Total joint replacement devices* (pp. 147–163). ASTM international (West Conshohocken, PA: ASTM International, 2015).
- Dienwiebel M, de Barros Bouchet, M-I. *Advanced analytical methods in tribology*. Cham: Springer International Publishing; 2018.
- Drynda, S., Drynda, A., Feuerstein, B., Kekow, J., Lohmann, C. H., & Bertrand, J. (2018). The effects of cobalt and chromium ions on transforming growth factor-beta patterns and mineralization in human osteoblast-like MG63 and SaOs-2 cells. *Journal of Biomedical Materials Research. Part A*, 106, 2105–2115.
- Eckert, J. A., Mueller, U., Jaeger, S., Panzram, B., & Kretzer, J. P. (2016). Fretting and corrosion in modular shoulder arthroplasty: A retrieval analysis. *BioMed Research International*, 2016, 1695906:1–1695906:7.
- Fevang, B. T. S., Nystad, T. W., Skredderstuen, A., Furnes, O. N., & Havelin, L. I. (2015). Improved survival for anatomic total shoulder prostheses. *Acta Orthopaedica*, 86, 63–70.
- Gilbert, J. L., Buckley, C. A., & Jacobs, J. J. (1993). In vivo corrosion of modular hip prosthesis components in mixed and similar metal combinations. The effect of crevice, stress, motion, and alloy coupling. *Journal of Biomedical Materials Research*, 27, 1533–1544.
- Gilbert, J. L., Mali, S. A., & Sivan, S. (2015). Corrosion of modular tapers in total joint replacements: A critical assessment of design, materials, surface structure, mechanics, electrochemistry, and biology. In A. S. Greenwald, S. M. Kurtz, J. E. Lemons, & W. M. Mihalko (Eds.), *Modularity and tapers in total joint replacement devices* (pp. 192–223). ASTM international (West Conshohocken, PA: ASTM International, 2015).
- Gilbert, J. L., Sivan, S., Liu, Y., Kocagöz, S. B., Arnholt, C. M., & Kurtz, S. M. (2015). Direct in vivo inflammatory cell-induced corrosion of CoCrMo alloy orthopedic implant surfaces. *Journal of Biomedical Materials Research. Part A*, 103, 211–223.
- Goldberg, J. R., Buckley, C. A., Jacobs, J. J., & Gilbert, J. L. (1997). Corrosion testing of modular hip implants. In D. E. Marlowe, J. E. Parr, & M. B. Mayor (Eds.), *Modularity of orthopedic implants* (pp. 157–176). ASTM international (West Conshohocken, PA: ASTM International, 1997).
- Goldberg, J. R., Gilbert, J. L., Jacobs, J. J., Bauer, T. W., Paprosky, W., & Leurgans, S. (2002). A multicenter retrieval study of the taper interfaces of modular hip prostheses. *Clinical Orthopaedics and Related Research*, 401, 149–161.
- Grupp, T. M., Weik, T., Bloemer, W., & Knaebel, H.-P. (2010). Modular titanium alloy neck adapter failures in hip replacement—Failure mode analysis and influence of implant material. *BMC Musculoskeletal Disorders*, 11, 3.
- Hall, D. J., Pourzal, R., Lundberg, H. J., Mathew, M. T., Jacobs, J. J., & Urban, R. M. (2018). Mechanical, chemical and biological damage modes within head-neck tapers of CoCrMo and Ti6Al4V contemporary hip replacements. *Journal of Biomedical Materials Research. Part B, Applied Biomaterials*, 106, 1672–1685.
- Hallab, N. J., Anderson, S., Caicedo, M., Skipor, A., Campbell, P., & Jacobs, J. J. (2004). Immune responses correlate with serum-metal in metal-on-metal hip arthroplasty. *The Journal of Arthroplasty*, 19, 88–93.
- Herrera, M., Espinoza, A., Méndez, J., Castro, M., López, J., & Rendón, J. (2005). Effect of C content on the mechanical properties of solution treated as-cast ASTM F-75 alloys. *Journal of Materials Science. Materials in Medicine*, 16, 607–611.
- Higgs, G. B., Hanzlik, J. A., MacDonald, D. W., Gilbert, J. L., Rinnac, C. M., & Kurtz, S. M. (2013). Is increased modularity associated with increased fretting and corrosion damage in metal-on-metal total hip arthroplasty devices?: A retrieval study. *The Journal of Arthroplasty*, 28, 2–6.
- Hussey, D. K., & McGrory, B. J. (2017). Ten-year cross-sectional study of mechanically assisted crevice corrosion in 1352 consecutive patients with metal-on-polyethylene total hip arthroplasty. *The Journal of Arthroplasty*, 32, 2546–2551.
- Jenko, M., Gorenšek, M., Godec, M., Hodnik, M., Batič, B. Š., Donik, Č., John, T. G., & Drago, D. (2018). Surface chemistry and microstructure of metallic biomaterials for hip and knee endoprostheses. *Applied Surface Science*, 427, 584–593.
- Karpuschewski, B., Pieper, H. J., Krause, M., & Döring, J. (2013). CoCr is Not the same: CoCr-blanks for dental machining. In G. Schuh, R. Neugebauer, & E. Uhlmann (Eds.), *Future trends in production engineering* (Vol. 44, pp. 261–274). Berlin: Springer.
- Khair, M. M., Nam, D., DiCarlo, E., & Su, E. (2013). Aseptic lymphocyte dominated Vasculitis-associated lesion resulting from trunnion corrosion in a cobalt-chrome unipolar hemiarthroplasty. *The Journal of Arthroplasty*, 28, 196.e11–196.e14.
- Kim, S. H., Wise, B. L., Zhang, Y., & Szabo, R. M. (2011). Increasing incidence of shoulder arthroplasty in the United States. *The Journal of Bone and Joint Surgery. American Volume*, 93, 2249–2254.
- Klutzny, M., Singh, G., Hameister, R., Goldau, G., Awiszus, F., Feuerstein, B., ... Lohmann, C. H. (2019). Screw track osteolysis in the cementless total knee replacement design. *The Journal of Arthroplasty*, 34, 965–973.
- Kurtz, S., MacDonald, D., Gilbert, J., Mont, M., Klein, G., Chen, A., et al. (2015). Is taper fretting corrosion a threat to the clinical performance of large-diameter hips with highly crosslinked polyethylene bearings? In A. S. Greenwald, S. M. Kurtz, J. E. Lemons, & W. M. Mihalko (Eds.), *Modularity and tapers in total joint replacement devices* (pp. 45–58). ASTM international (West Conshohocken, PA: ASTM International, 2015).
- Kurtz, S. M., MacDonald, D. W., Gilbert, J. L., Mont, M. A., Klein, G., Klein, G., Chen, A., Kraay, M., Hamlin, B., & Rinnac, C. M. (2013). Do ceramic femoral heads reduce taper fretting corrosion in hip arthroplasty? A retrieval study. *Clinical Orthopaedics and Related Research*, 471, 3270–3282.
- Lin, H.-Y., & Bumgardner, J. D. (2004). In vitro biocorrosion of Co-Cr-Mo implant alloy by macrophage cells. *Journal of Orthopaedic Research*, 22, 1231–1236.
- Liu, Y., & Chen, B. (2018). In vivo corrosion of CoCrMo alloy and biological responses: A review. *Materials Technology*, 33, 127–134.
- Lundberg, H. J., Ha, N. Q., Hall, D. J., Urban, R. M., Levine, B. R., & P. R. (2015). Contact mechanics and plastic deformation at the local surface topography level after assembly of modular head-neck junctions in modern total hip replacement devices. In A. S. Greenwald, S. M. Kurtz, J. E. Lemons, & W. M. Mihalko (Eds.), *Modularity and tapers in total*

- joint replacement devices (pp. 59–82). ASTM international (West Conshohocken, PA: ASTM International, 2015).
- McGrory, B. J., MacKenzie, J., & Babikian, G. (2015). A high prevalence of corrosion at the head-neck taper with contemporary Zimmer non-cemented femoral hip components. *The Journal of Arthroplasty*, *30*, 1265–1268.
- Meyer, H., Mueller, T., Goldau, G., Chamaon, K., Ruetschi, M., & Lohmann, C. H. (2012). Corrosion at the cone/taper interface leads to failure of large-diameter metal-on-metal total hip arthroplasties. *Clinical Orthopaedics and Related Research*, *470*, 3101–3108.
- Mueller, U., Braun, S., Schroeder, S., Sonntag, R., & Kretzer, J. P. (2017). Same same but different? 12/14 stem and head tapers in Total hip Arthroplasty. *The Journal of Arthroplasty*, *32*, 3191–3199.
- National Joint Replacement Registry. 2016. *Hip, knee & shoulder arthroplasty: Annual report*. Australian Orthopaedic Association.
- Neer, C. S., Watson, K. C., & Stanton, F. J. (1982). Recent experience in total shoulder replacement. *The Journal of Bone and Joint Surgery. American Volume*, *64*, 319–337.
- Panagiotidou, A., Meswania, J., Hua, J., Muirhead-Allwood, S., Hart, A., & Blunn, G. (2013). Enhanced wear and corrosion in modular tapers in total hip replacement is associated with the contact area and surface topography. *Journal of Orthopaedic Research*, *31*, 2032–2039.
- Plummer, D. R., Berger, R. A., Paprosky, W. G., Sporer, S. M., Jacobs, J. J., & Della Valle, C. J. (2016). Diagnosis and management of adverse local tissue reactions secondary to corrosion at the head-neck junction in patients with metal on polyethylene bearings. *The Journal of Arthroplasty*, *31*, 264–268.
- Pourzal, R., Hall, D. J., Ehrich, J., McCarthy, S. M., Mathew, M. T., Jacobs, J. J., & Urban, R. M. (2017). Alloy microstructure dictates corrosion modes in THA modular junctions. *Clinical Orthopaedics and Related Research*, *475*, 3026–3043.
- Pourzal, R., Hall, D. J., Ha, N. Q., Urban, R. M., Levine, B. R., Jacobs, J. J., & Lundberg, H. J. (2016). Does surface topography play a role in taper damage in head-neck modular junctions? *Clinical Orthopaedics and Related Research*, *474*, 2232–2242.
- Rasmussen, J. V., Hole, R., Metlie, T., Brorson, S., Äärämaa, V., Demir, Y., ... Jensen, S. L. (2018). Anatomical total shoulder arthroplasty used for glenohumeral osteoarthritis has higher survival rates than hemiarthroplasty: A Nordic registry-based study. *Osteoarthritis and Cartilage*, *26*, 659–665.
- Rehmer, A., Bishop, N. E., & Morlock, M. M. (2012). Influence of assembly procedure and material combination on the strength of the taper connection at the head-neck junction of modular hip endoprostheses. *Clinical Biomechanics*, *27*, 77–83.
- Schwachmeyer, V., Damm, P., Bender, A., Dymke, J., Graichen, F., & Bergmann, G. (2013). In vivo hip joint loading during post-operative physiotherapeutic exercises. *PLoS One*, *8*(e77807), 1–8.
- Singh, J. A., Sperling, J. W., & Cofield, R. H. (2011). Revision surgery following total shoulder arthroplasty: Analysis of 2588 shoulders over three decades (1976 to 2008). *Journal of Bone and Joint Surgery. British Volume (London)*, *93*, 1513–1517.
- Sperling, J. W., Cofield, R. H., O'Driscoll, S. W., Torchia, M. E., & Rowland, C. M. (2000). Radiographic assessment of ingrowth total shoulder arthroplasty. *Journal of Shoulder and Elbow Surgery*, *9*, 507–513.
- Stemmer, P., & Fischer, A. (2018). Pathways of dissipation of frictional energy under boundary lubricated sliding Wear of martensitic materials. *Lubricants*, *6*, 34.
- Teeter, M. G., Carroll, M. J., Walch, G., & Athwal, G. S. (2016). Tribocorrosion in shoulder arthroplasty humeral component retrievals. *Journal of Shoulder and Elbow Surgery*, *25*, 311–315.
- Weeton JW, Signorelli RA. 1954. An investigation of lamellar structures and minor phases in eleven cobalt-base alloys before and after heat treatment. NACA TN 3109.
- Westerhoff, P., Graichen, F., Bender, A., Halder, A., Beier, A., Rohlmann, A., & Bergmann, G. (2009). In vivo measurement of shoulder joint loads during activities of daily living. *Journal of Biomechanics*, *42*, 1840–1849.

SUPPORTING INFORMATION

Additional supporting information may be found online in the Supporting Information section at the end of this article.

How to cite this article: Crackau M, Märtens N, Harnisch K, et al. In vivo corrosion and damages in modular shoulder prostheses. *J Biomed Mater Res*. 2020;108B:1764–1778. <https://doi.org/10.1002/jbm.b.34519>